

Tessellated Wasserstein Auto-Encoders

Kuo Gai and Shihua Zhang*

Abstract—Non-adversarial generative models such as variational auto-encoder (VAE), Wasserstein auto-encoders with maximum mean discrepancy (WAE-MMD), sliced-Wasserstein auto-encoder (SWAE) are relatively easy to train and have less mode collapse compared to Wasserstein auto-encoder with generative adversarial network (WAE-GAN). However, they are not very accurate in approximating the target distribution in the latent space because they don't have a discriminator to detect the minor difference between real and fake. To this end, we develop a novel non-adversarial framework called Tessellated Wasserstein Auto-encoders (TWAE) to tessellate the support of the target distribution into a given number of regions by the centroidal Voronoi tessellation (CVT) technique and design batches of data according to the tessellation instead of random shuffling for accurate computation of discrepancy. Theoretically, we demonstrate that the error of estimate to the discrepancy decreases when the numbers of samples n and regions m of the tessellation become larger with rates of $\mathcal{O}(\frac{1}{\sqrt{n}})$ and $\mathcal{O}(\frac{1}{\sqrt{m}})$, respectively. Given fixed n and m , a necessary condition for the upper bound of measurement error to be minimized is that the tessellation is the one determined by CVT. TWAE is very flexible to different non-adversarial metrics and can substantially enhance their generative performance in terms of Fréchet inception distance (FID) compared to VAE, WAE-MMD, SWAE. Moreover, numerical results indeed demonstrate that TWAE is competitive to the adversarial model WAE-GAN, demonstrating its powerful generative ability.

Index Terms—Non-adversarial generative models, Wasserstein auto-encoder, centroidal Voronoi tessellation, sphere packing, optimal transportation, optimization with non-identical batches



1 INTRODUCTION

Knowing the distribution of data is a fundamental task of data science. Prior distributions such as Laplacian, Gaussian and Gaussian mixture distributions are often utilized to model the data. However, their ability of representation is limited. With the rise of deep learning, we can use more parameters to model the distribution accurately. The basic assumption of such methods is that complex high-dimensional data such as images concentrate near a low-dimensional manifold. Generative adversarial network (GAN) [1] and Wasserstein auto-encoder with generative adversarial network (WAE-GAN) (also known as adversarial auto-encoder (AAE)) [2] [3] are the representatives and have many variants. GAN trains a generator to generate new samples and a discriminator to teach the generator to improve its quality. From a probabilistic view, the generator maps points from a simple low-dimensional distribution such as a uniform distribution or a Gaussian distribution to the target high-dimensional distribution (e.g., face or handwriting images), while the discriminator computes the discrepancy between the generated distribution and the target one. WAE-GAN trains an invertible mapping between two distributions with the Wasserstein distance as the reconstruction loss, i.e., an encoder from the data space to the latent space and a decoder from the latent space to the data space. WAE-GAN employs GAN to minimize the discrepancy between the output of the encoder and the samplable prior distribution in the latent space. Both

methods utilize adversarial training, i.e., a two player game between generator (encoder) and discriminator.

As we know that GAN is hard to train. Arjovsky *et al.* [4] [5] ascribed this to the choice of discrepancy. Classification GAN utilizes KL-divergence and performs good under some tricks [6]. But in theory, when the supports of two distributions are disjoint, KL-divergence fails and causes instability of the model. A more stable variant Wasserstein-GAN (WGAN) introduced from the optimal transportation view utilizes a discriminator with clipped parameters to compute the Wasserstein distance. However, clipping limits the discriminator to find the subtle difference between two distributions. Another strategy imposes the one-Lipschitz constraint by regularization methods. Since the Wasserstein distance is a real distance, the optimization appears more stable and converges faster than GAN. Apart from the optimal transportation, several other studies have also been proposed to explain and improve this [6] [7] [8] [9].

The complexity of high-dimensional data and the instability of adversarial models lead to mode collapse, which is the main obstacle for GANs in many applications. The mode collapse in GANs refers to the problem of overfitting to a part of the training modes and forget the rest. Lucic *et al.* [10] showed that even the best GAN dropped 72% of the modes. In theory, Arora *et al.* [11] proved that the trained distribution will not converge to the target one with several standard metrics. This can be blamed on the adversarial mechanism. In game theory, based on gradient descent optimization algorithm, the discriminator and generator find a local Nash equilibrium rather than a global one. From a statistical view, the discriminator has cumulative preference of mode when it classifies real and fake data in the training process, since the discriminator is trained based on the former step. So the discriminator is sensitive to some modes and insensitive to others. More formally,

• Kuo Gai and Shihua Zhang are with the NCMIS, CEMS, RSCDS, Academy of Mathematics and Systems Science, Chinese Academy of Sciences, Beijing 100190, School of Mathematical Sciences, University of Chinese Academy of Sciences, Beijing 100049, and Center for Excellence in Animal Evolution and Genetics, Chinese Academy of Sciences, Kunming 650223, China.

*To whom correspondence should be addressed. Email: zsh@amss.ac.cn.

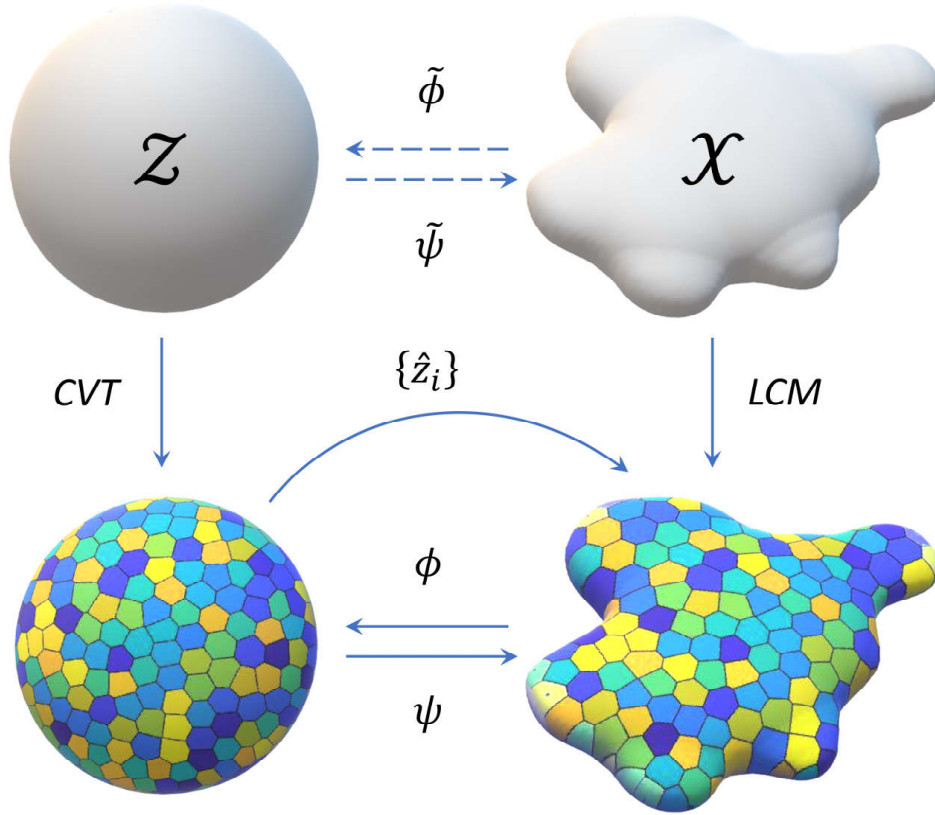


Fig. 1. Illustration of TWAE. In a traditional way, the encoder $\tilde{\phi} : \mathcal{X} \rightarrow \mathcal{Z}$ and decoder $\tilde{\psi} : \mathcal{Z} \rightarrow \mathcal{X}$ are trained using randomly shuffled batches of data. In TWAE, the support of a known distribution is tessellated by the centroidal Voronoi tessellation (CVT) procedure, then the batch of data is designed with the least cost method (LCM) by their distance to the centroid $\{\hat{z}_i\}$ of each region. In the end, the auto-encoder (ϕ, ψ) is trained over region by region.

the estimation of discrepancy is biased, which makes the generated distribution not converge to the target one.

To solve this problem, a potential approach is to find alternatives of the adversarial mechanism by computing the discrepancy without neural network for discrimination. For example, a kernel-based method maximum mean discrepancy (MMD) shows a good property on approximating the independent and identically distributed (i.i.d.) Gaussian distribution and finds its usage on WAE-MMD [3] and MMD-GAN [12]. However, MMD only matches principle features of two distributions and lose other ones which cannot be captured by the kernel. As to the discrepancy of arbitrary distributions, researchers have introduced a new metric called the sliced-Wasserstein (SW) distance [13], which has similar qualitative properties with the Wasserstein distance. But it is much easier to compute. Inspired by the one-dimensional case of the Wasserstein distance, the data is projected onto an one-dimensional subspace for analytical solution, then the SW distance is obtained by integrating over all the subspaces. Thus, the number of samples needed to estimate the integration increases as the dimension of data goes up.

Compared to adversarial training, non-adversarial approaches have no cumulative preference since they do not utilize historical information and are easy to train due to the unemployment of the discriminator. However, since the distribution of high-dimensional data concentrates near a low-dimensional manifold, where the Euclidean distance

is no longer effective, non-adversarial approaches are not over-parameterized to learn the distance on the manifold. So they may be cursed by high dimensionality. This means, when the dimension is high and the shape of the manifold is complicated, the error of the estimation to the discrepancy may be beyond tolerance. As a consequence, the performance of non-adversarial algorithms such as VAE, WAE-MMD, SWAE are not as good as that of WAE-GAN or variants of GAN under similar architectures of neural network.

In this paper, we develop a novel non-adversarial framework—Tessellated Wasserstein Auto-encoders (TWAE) to tessellate the support of the target distribution in the latent space into a given number of regions and design batches of data according to the tessellation instead of random shuffling. In more detail, the cost function of classical generative auto-encoders consists of the reconstruction error in the data space and the discrepancy error in the latent space. To compute the latter, TWAE separates the computation of the global discrepancy into some local ones. To do this, we need to obtain a tessellation of the support of both the generated and target distributions (Fig. 1). We implement this task in two steps: first we tessellate the support of the prior distribution; second we cluster the encoded data corresponding to the tessellation in the first step. For the first step, we provide two ways to achieve the tessellation: centroidal Voronoi tessellation (CVT) and sphere packing. CVT can generate points which are the centroids of the

corresponding Voronoi regions. Asymptotically speaking, all regions of the optimal CVT are congruent to a basic region. CVT can be applied to a connected set in R^n with arbitrary shapes. The sphere packing approach can tessellate the space into exactly congruent regions with E_8 -lattice in R^8 and Leech lattice in R^{24} . For the second step, we adopt an assignment algorithm to keep the correspondence of the real data and the generated one. Thereby the discrepancy on the whole support is separated into a sum of local discrepancies on each region. Compared with traditional ways of sampling on the whole support, TWAE can sample more points in each region. Thus, we can force the generated distribution to approximate the target one better. Since the tessellation is independent of the choice of discrepancy metrics, TWAE is compatible to different metrics and enhance their performance.

The rest of this paper is organized as follows. In section 2, we start from the optimal transportation and briefly review the optimal transportation-based generative methods such as WGAN [4], SWGAN [14] and WAE [3]. To the end, we introduce CVT and sphere packing as basic tools to achieve the tessellation. In section 3, we describe TWAE in details. In section 4, we derive the sample and measurement error of TWAE theoretically. In section 5, we conduct extensive experiments to demonstrate the effectiveness of TWAE. In section 6, we provide discussion and conclusion.

2 RELATED WORK

2.1 Optimal transportation

The optimal transportation problem stems from a problem on transporting commodities. Suppose there are m sources x_1, \dots, x_m for a commodity, with a_i units of supply at x_i and n sinks y_1, \dots, y_n for it, with b_i units of demand at y_i , c_{ij} ($i = 1, \dots, m; j = 1, \dots, n$) is the cost of transporting one unit of this commodity from x_i to y_j . We wish to find a transportation plan $\{f_{ij} | i = 1, \dots, m; j = 1, \dots, n\}$ to minimize the total cost. The problem can be formulated as

$$\begin{aligned} \min \quad & \sum_{i,j} c_{ij} f_{ij} \\ \text{s.t.} \quad & \sum_{j=1}^n f_{ij} = a_i, \quad i = 1, \dots, m \\ & \sum_{i=1}^m f_{ij} = b_j, \quad i = 1, \dots, n \\ & f_{ij} \geq 0 \end{aligned} \quad (1)$$

which can be solved by linear programming.

With the development of measure theory, the transportation problem can be stated as follows [15]

$$W_c(P_x, P_y) = \inf_{\mathcal{T}} \mathbb{E}_{x \sim P_x} [c(x, \mathcal{T}(x))] \quad (2)$$

where $\mathcal{T} : X \rightarrow Y$ is a measure preserving transformation. There can be no admissible \mathcal{T} , for instance if P_x is a Dirac delta and P_y is not. To overcome this difficulty, Kantorovich [16] proposed the following way to relax this problem

$$W_c(P_x, P_y) = \inf_{\Gamma \in \Pi(P_x, P_y)} \mathbb{E}_{(x,y) \sim \Gamma} [c(x, y)] \quad (3)$$

where $\Pi(P_x, P_y)$ denotes the set of all joint distributions $\Gamma(x, y)$ whose marginals are respectively P_x and P_y . $c : X \times$

$Y \rightarrow [0, \infty]$ is the cost function of transporting. Intuitively, $\Gamma(x, y)$ indicates how much “mass” must be transported from x to y in order to transform the distribution P_x into the distribution P_y . The infimum of the transportation cost is called the Wasserstein distance of two distributions P_x and P_y . The Wasserstein distance is a true distance and has a finer topology to guarantee convergence when minimize the distance. But the Wasserstein distance is hard to compute because the feasible region of $\Pi(P_x, P_y)$ is too large to search. If the two distributions are assumed to be Gaussian, i.e., $x \sim \mathcal{N}(m_1, \Sigma_1)$, $y \sim \mathcal{N}(m_2, \Sigma_2)$ with the means $m_1, m_2 \in \mathbb{R}^p$ and the covariance $\Sigma_1, \Sigma_2 \in \mathbb{R}^{p \times p}$, their squared Wasserstein distance has a closed form [17]

$$\begin{aligned} GW^2 = W_2^2(P_x, P_y) = & \|m_1 - m_2\|_2^2 \\ & + \text{tr} \left(\Sigma_1 + \Sigma_2 - 2 \left(\Sigma_2^{1/2} \Sigma_1 \Sigma_2^{1/2} \right)^{1/2} \right) \end{aligned} \quad (4)$$

This is denoted as the GW distance.

2.2 Optimal transportation-based generative models

Arjovsky *et al.* [4] first approached the problem of generative modeling from the optimal transportation view. The infimum in (2) is highly intractable. On the other hand, the Kantorovich-Rubinstein duality [18] tells us that

$$W_1(P_x, P_y) = \sup_{\|f\|_L \leq 1} (\mathbb{E}_{x \sim P_x} [f(x)] - \mathbb{E}_{y \sim P_y} [f(y)]) \quad (5)$$

where the supremum is over all the one-Lipschitz functions $\{f : \mathcal{X} \rightarrow \mathbb{R}\}$. The function f is approximated by a parameterized family of functions $\{f_w\}_{w \in \mathcal{W}}$. Arjovsky *et al.* [4] suggested to impose the one-Lipschitz constraint to force parameters w lie in a compact space by clipping the weights to a fixed box. Gulrajani *et al.* [19] introduced a soft version of the constraint with a penalty on the gradient norm for random samples by optimizing

$$L = \mathbb{E}_{x \sim P_x} [f(x)] - \mathbb{E}_{y \sim P_y} [f(y)] + \lambda \mathbb{E}_{\hat{x} \sim P_{\hat{x}}} [(\|\nabla_{\hat{x}} f(\hat{x})\|_2 - 1)^2] \quad (6)$$

To improve the stability of WGAN, Deshpande *et al.* [14] developed a mechanism based on random projections as an alternative to the black-box discriminator. Notice that the squared Wasserstein distance of two one-dimensional distributions P_x and P_y can be estimated accurately by sorting their samples according to their values. Suppose x_i, y_i ($i = 1, \dots, N$) are independently sampled from P_x and P_y , and $x_i \leq x_{i+1}, y_i \leq y_{i+1}$ for all $i \in \{1, \dots, N-1\}$, then

$$W_2^2(P_x, P_y) \approx \frac{1}{N} \sum_{i=1}^N (x_i - y_i)^2 \quad (7)$$

Generally, if P_x and P_y are d -dimensional distributions, we project the sampled d -dimensional points onto one-dimensional spaces spanned by directions w and integrate over all possible directions w on the unit sphere S^{d-1} . Then we obtain the SW distance

$$SW_2^2(P_x, P_y) = \int_{w \in S^{d-1}} W_2^2(P_{x|w}, P_{y|w}) dw \quad (8)$$

Hereby $P_{x|w}$ and $P_{y|w}$ denote the projected distribution on the subspace spanned by w . The SW distance is a real

distance and is equivalent to the Wasserstein distance as the following property holds [13]

$$SW_2^2(P_x, P_y) \leq C_d W_2^2(P_x, P_y) \leq C_d R^{\frac{1}{d+1}} SW_2^{\frac{1}{d+1}}(P_x, P_y) \quad (9)$$

where $C_d > 0$ is a constant correlated with the dimension d , and $P_x, P_y \in \mathcal{P}(B(0, R))$, where $B(0, R)$ is the ball with radius R and the origin as the center point, $\mathcal{P}(\cdot)$ is the space of probability measure. The SW distance can be regarded as a good alternative to the Wasserstein distance because it can be easily acquired by random projections. However, since the area of a sphere with a radius of r in \mathbb{R}^d is proportional to r^{d-1} , the number of projections goes up exponentially with the dimension of data. Hence, the huge computation caused by the curse of dimensionality becomes a main obstacle to put it into practice. The SW-based methods sacrifice accuracy to the discrepancy for the privilege of stability without the discriminator.

Another main stream of generative models is based on auto-encoders. Different from GAN, generative auto-encoders approximate a prior distribution in the latent space. Their generalized formulation is as follows

$$\min_{\phi, \psi} \mathbb{E}_{x \sim P_x} [c(x, \psi(\phi(x)))] + \lambda D(P_z || Q_z) \quad (10)$$

where ϕ is the encoder, ψ is the decoder, P_x is the data distribution, P_z is a prior samplable distribution, Q_z is the empirical distribution of the encoded data $z = \phi(x)$, and λ indicates the relative importance of the discrepancy. In WAE [3], GAN and MMD have been proposed (denoted as WAE-GAN and WAE-MMD respectively). In SWAE [20], the choice of D in (10) is the SW distance.

2.3 Centroidal Voronoi Tessellation

Given an open set $\Omega \subseteq \mathbb{R}^d$, the set $\{V_i\}_{i=1}^k$ is called a tessellation of Ω if $V_i \cap V_j = \emptyset$ for $i \neq j$ and $\cup_{i=1}^k \bar{V}_i = \bar{\Omega}$ ($\bar{\Omega}$ means the closed hull of set Ω). Given a set of points $\{\hat{z}_i\}_{i=1}^k$ belonging to $\bar{\Omega}$, the set $\{\hat{V}_i\}_{i=1}^k$ is called a Voronoi tessellation if the Voronoi region \hat{V}_i corresponding to the point \hat{z}_i is defined by

$$\hat{V}_i = \{x \in \Omega | \|x - \hat{z}_i\| < \|x - \hat{z}_j\| \text{ for } j = 1, \dots, k, j \neq i\} \quad (11)$$

The points $\{\hat{z}_i\}_{i=1}^k$ are called generators. In the rest of this paper, without special mention, a generator denotes the generator of tessellation rather than that of GAN. Given a region $V \subseteq \mathbb{R}^d$ and a density function ρ , the mass centroid z^* of V is defined by

$$z^* = \frac{\int_V y \rho(y) dy}{\int_V \rho(y) dy} \quad (12)$$

If $\hat{z}_i = z_i^*$, $i = 1, \dots, k$, i.e., the mass centroid of the region is exactly the generator, we call such a tessellation a CVT [21].

Next, we introduce the classical Lloyd's method to construct an approximate CVT in the following steps: **Step 0**: Select an initial set of k points $\{z_i\}_{i=1}^k$ using a sampling strategy (e.g., Monte Carlo sampling); **Step 1**: Construct the Voronoi tessellation $\{V_i\}_{i=1}^k$ of Ω associated with the points $\{z_i\}_{i=1}^k$; **Step 2**: Compute the mass centroids of the Voronoi regions $\{V_i\}_{i=1}^k$ found in **Step 1**; these centroids are the

new set of points $\{z_i\}_{i=1}^k$; **Step 3**: If this new set of points meets some convergence criteria, then terminate; otherwise, return to **Step 1**. The Lloyd's method can be viewed as an alternative iteration between the Voronoi tessellation construction and centroid computation. Clearly, a CVT is a fixed point of the iteration.

2.4 Sphere Packing

The CVT technique is an approximate method. In mathematics, there is an exact method based on sphere packing to tessellate the space. The standard packing problem is how to arrange spheres of equal radius to fill space as densely as possible in \mathbb{R}^n . It is very hard to construct a packing scheme for an arbitrary n . Luckily, for the special cases, it has been proved that E_8 -lattice ($n = 8$) and Leech lattice ($n = 24$) give the densest lattice packing [22]. For E_8 -lattice, each lattice point has 240 nearest neighbors, and for Leech lattice the number is 196560 which is too large for our tessellation considering the sizes of common data. In more detail, for E_8 -lattice, the nearest neighbors of the origin have the shape $(\pm 1^2, 0^6)$ ($2^2 C_8^2 = 112$ of these) and $(\pm \frac{1}{2}^8)$ with even number of negative signs ($2^7 = 128$ of these). The set of neighbors Δ is actually the root lattice of E_8 -lattice since $E_8 = \mathbb{Z}\Delta$.

Though E_8 gives the densest packing in \mathbb{R}^8 , it may not be optimal restricted to a region with a fixed shape. Nevertheless, for a ball B in \mathbb{R}^8 , a possible tessellation scheme utilizing E_8 -lattice is that one point locates at the center of B , surrounded by 240 points in the way of E_8 within B . By adjusting the radius of packed spheres, we obtain a tessellation for B , which is symmetrical and has regions with exactly the same volume. Then if we tessellate the space with the tangent plane of each two spheres, we separate the space into regions with exactly the same volume rather than roughly equal one in a CVT.

3 TWAE

3.1 Model Construction

We follow the generalized formulation of generative auto-encoder with a reconstruction error in the data space and a discrepancy error in the latent space,

$$\min_{\phi, \psi} \mathbb{E}_{x \sim P_x} [c(x, \psi(\phi(x)))] + \lambda D(P_z || Q_z) \quad (13)$$

In this paper, we propose P_z to be a uniform distribution in a unit ball, then the probability of a region is proportional to its volume. We adopt the Wasserstein distance as the divergence D for its good property though our tessellation framework is also flexible to other discrepancy metrics.

Let's go back to the discrete Wasserstein distance (1). Suppose there are N points of \tilde{z}_i sampled from the prior distribution P_z and the same number of z_i encoded by the encoder ϕ . P_N and Q_N are the empirical distribution of $\{\tilde{z}_i\}_{i=1}^N$ and $\{z_i\}_{i=1}^N$, respectively. We can compute the Wasserstein distance by assigning each z_i to a \tilde{z}_{σ_i} as follows

$$W(P_N, Q_N) = \frac{1}{N} \min_{\sigma} \sum_{i=1}^N \|z_i - \tilde{z}_{\sigma_i}\| \quad (14)$$

where σ is a permutation of an index set $\{1, \dots, N\}$. It can be formulated as an assignment problem and solved

by mature linear programming algorithms with a computational complexity of $O(N^{2.5}\log(N))$. This complexity is prohibitive for usage in the inner loop of a learning algorithm. As mentioned before, instead of linear programming, inaccurate approaches such as clipped networks [4] and random projection [14] have been proposed to address it. For large N , the traditional way is to divide the dataset into batches and to optimize the objective function batch by batch in a gradient descent manner, which is the well-known stochastic gradient descent. However, batches with small size lose some information to model the distribution delicately. To address this issue, we combine the assignment method and the batch optimization to a two-step algorithm. That is we first design the batches according to their similarity and then minimize the discrepancy based on the optimization per batch.

For the first step, we find m points $\{\hat{z}_j\}_{j=1}^m$ on the support of P_z . $\{\hat{z}_j\}_{j=1}^m$ can be treated as generators of a tessellation $\{V_j\}_{j=1}^m$ on the support Ω that $V_i \cap V_j = \emptyset$ for $i \neq j$ and $\cup_{i=1}^m V_i = \Omega$. We assume that the volume of each V_j is equal so that we can sample a batch with the same number n of points in each V_j to model the distribution of P_z restricted on V_j . Assigning each encoded data point z_i to one of the generators $\{\hat{z}_j\}_{j=1}^m$ is an easier task than (14) because m is much smaller than N . Each of $\{\hat{z}_j\}_{j=1}^m$ is assigned by $n = \frac{N}{m}$ points. The problem can be formulated as

$$\begin{aligned} \min \quad & \sum_{i,j} \|z_i - \hat{z}_j\|_2^2 f_{ij} \\ \text{s.t.} \quad & \sum_{j=1}^m f_{ij} = 1, \quad i = 1, \dots, N \\ & \sum_{i=1}^N f_{ij} = n, \quad j = 1, \dots, m \\ & f_{ij} \in \{0, 1\} \end{aligned} \quad (15)$$

It is a special case of the Hitchcock problem as both the demands and supplies are equal. By doing this, the dataset $\{z_i\}_{i=1}^N$ is clustered into m sets $\{S_j\}_{j=1}^m$ according to their distance to the generators $\{\hat{z}_j\}_{j=1}^m$. Then for each cluster S_j corresponding to the generator \hat{z}_j , we can estimate the Wasserstein distance of Q_z and P_z restricted on the region V_j .

The overall discrepancy is obtained by computing the local ones upon all the sets $\{S_j\}_{j=1}^m$. Thus, we have

$$\mathbb{E}[W_2^2(P_N, Q_N)] = \frac{1}{N} \mathbb{E} \left[\min_{\sigma} \sum_{i=1}^N \|z_i - \tilde{z}_{\sigma_i}\|_2^2 \right] \quad (16)$$

$$= \frac{1}{N} \mathbb{E} \left[\min_{\sigma} \sum_{j=1}^m \sum_{z_i \in S_j} \|z_i - \tilde{z}_{\sigma_i}\|_2^2 \right] \quad (17)$$

$$\leq \frac{1}{N} \mathbb{E} \left[\sum_{j=1}^m \min_{\sigma_j} \sum_{\substack{z_i \in S_j \\ \tilde{z}_{\sigma_i^j} \in V_j}} \|z_i - \tilde{z}_{\sigma_i^j}\|_2^2 \right] \quad (18)$$

$$= \frac{1}{m} \mathbb{E} \left[\sum_{j=1}^m W(P_{n|V_j}, Q_{n|S_j}) \right] \quad (19)$$

Algorithm 1 TWAE

Input: data $\{x_i\}_{i=1}^N$, CVT generators $\{\hat{z}_i\}_{i=1}^m$, hyperparameter λ

Output: encoder ϕ , decoder ψ

```

1: repeat
2:    $z_i = \phi(x_i), i \in \{1, \dots, N\}$ 
3:   assign  $\{z_i\}$  to  $\{\hat{z}_i\}$  by Algorithm 2 and obtain  $\{S_i\}_{i=1}^m$ 
4:   for  $k = 1 \rightarrow m$  do
5:     sample  $n$  points  $\{z_s^k\}$  in the region  $V_k$ 
6:     compute  $\mathcal{L}_{latent}^k = W(P_{n|V_k}, Q_{n|S_k})$ 
7:      $\mathcal{L}_{recons}^k = \sum_{x \in \{x_t | z_t \in S_k\}} \|x - \psi(\phi(x))\|$ 
8:     update  $\phi$  and  $\psi$  by minimizing  $\mathcal{L}^k = \mathcal{L}_{recons}^k + \lambda \mathcal{L}_{latent}^k$ 
9:   end for
10: until convergence

```

where $P_{n|V_j}$ denotes the empirical distribution of n samples of P_z restricted on V_j , $Q_{n|S_j}$ denotes the empirical distribution of S_j , σ^j denotes a permutation of an index set $\{1, \dots, n\}$ corresponding to the region V_j . The inequation in (18) is because the solution of linear programming problem (15) may not agree with the true optimal transportation plan in (17). However, when $P_z = Q_z$, since S_j is a set of points which are the closest to \hat{z}_j , then for a fixed $z_i \in V_j$, its optimal match \tilde{z}_{σ_i} in (17) belongs to S_j with high probability. If we fix m and let N approach infinity, the equation holds in (18). We assume that in the training procedure, $N \gg m$ and after a few iterations, Q_z and P_z are approximately equal so that we can optimize the subproblems on the right side of (19) instead.

We expect the sum of errors of estimates to the local discrepancies is smaller than the error on the whole support with the same estimator. We assume the total error can be divided into measurement error e_m and sample error e_s . First, the measurement error denotes the error of the estimated Wasserstein distance. In general, the measurement error is a high-level minim of the true discrete Wasserstein distance. As the sum of estimations on the regions is almost equal to that on the whole support, the sum of measurement errors (e_m) on regions should be smaller. Second, traditionally, we sample a batch of points from the whole distribution, so fewer points locate in a region of the support. Now we sample a batch in a local region to find the more subtle discrepancy and approximate the prior distribution better. Thus, the sample error in local regions (e_s) is smaller. Our main results are that e_m and e_s decrease with rates of $\mathcal{O}(\frac{1}{\sqrt{m}})$ and $\mathcal{O}(\frac{1}{\sqrt{n}})$, respectively. We leave it to Section 4 for detailed theoretical exploration.

The whole scheme of the algorithm is summarized in **Algorithm 1**. Here we adopt the CVT technique to generate a proper tessellation. The volumes of regions are approximately equal. The Hitchcock problem needs to be solved in each iteration, and it still costs too much to find the optimal solution. We adopt the least cost method (LCM) instead, which is a heuristic algorithm. We find the smallest admissible item d_{ij}^* of the distance matrix between $\{z_i\}_{i=1}^N$ and $\{\hat{z}_j\}_{j=1}^m$, and assign z_i to \hat{z}_i if \hat{z}_i is not saturated. The scheme of LCM is summarized in **Algorithm 2**. As to the discrepancy, we propose two non-adversarial methods based on the GW distance (4) and the SW distance (8). Both discrepancy metrics can be computed efficiently.

Algorithm 2 LCM

Input: encoded data $\{z_i\}_{i=1}^N$, generators $\{\widehat{z}_i\}_{i=1}^m$,
Output: clusters $S_i, i = 1, \dots, m$
1: compute the distant matrix $M_{N \times m}$
2: $S_i = \emptyset, i = 1, \dots, m$
3: **repeat**
4: find the minimum item d_{ij} in M
5: $S_j = S_j \cup \{z_i\}$
6: mask the i_{th} row in M
7: **if** $|S_j| = n$ **then**
8: mask the j_{th} column in M
9: **end if**
10: **until** all of $\{z_i\}$ is assigned

3.2 Optimization with Non-identical Batches

Mini-batch gradient descent is the most common implementation of the gradient descent in the deep learning field. It splits the training data into small batches, which are used to calculate model error and update model coefficients. An underlying assumption of mini-batch gradient descent is that data in each batch are sampled from an identical distribution. Though the variance of empirical distribution increases with batch size becoming small, some techniques such as batch normalization and dropout enhance the robustness of the model. However, in our case, batches are designed with data from disjoint supports. The variance of designed batches is too large that it is beyond the tolerance of such techniques. So we adopt a new optimization method to make the algorithm converge to better solutions. Our main idea is to sample a batch randomly from the whole support to balance the variance induced by the designed batches.

The loss function f can be separated by batches

$$f(\theta) = \sum_{i=1}^m f_i(\theta) \quad (20)$$

where m is the number of batches, θ is the parameter of this model. The first-order Taylor expansion of $f_i(\theta)$ is

$$f_i(\theta) = f_i^{(1)}(\theta) + R_i(\theta) \quad (21)$$

where $f_i^{(1)}(\theta) = f_i(\bar{\theta}) + \nabla f_i(\bar{\theta})(\theta - \bar{\theta})$, $R_i(\theta) = f_i(\theta) - f_i^{(1)}(\theta)$. To assure the convergence while retaining the differences among batches, we let $f_i^{(1)}(\theta)$ stay the same and change $R_i(\theta)$ to $R(\theta)$, i.e., $f(\theta) - f^{(1)}(\theta)$. A hyper parameter α is added to keep the balance. Then when we optimize with the i th batch of data, we are actually optimizing

$$\min_{\theta} f_i^{(1)}(\theta) + \alpha R(\theta) \quad (22)$$

where $R(\theta)$ can be viewed as a regularizer. Since the popular optimization algorithms for deep learning are first-order gradient descent methods, we only need to concern about the gradient. For the k th iteration, the gradient we obtained from the objective function in (22) is

$$g = \nabla f_i(\theta_k) + \alpha(\nabla f(\theta_k) - \nabla f(\theta_{k-1})) \quad (23)$$

It is unrealistic to compute $\nabla f(\theta)$ as the number of data is huge. Actually, the only thing that matters is the variation $\nabla f(\theta_k) - \nabla f(\theta_{k-1})$, so we estimate $f(\theta_k)$ and $f(\theta_{k-1})$ with the same sampled data and compute the variation. This

Algorithm 3 TWAE with regularization

Input: data $\{x_i\}_{i=1}^N$, CVT generators $\{\widehat{z}_i\}_{i=1}^m$, hyperparameter λ, α
Output: encoder ϕ , decoder ψ
1: **repeat**
2: $z_i = \phi(x_i), i \in \{1, \dots, N\}$
3: assign $\{z_i\}$ to $\{\widehat{z}_i\}$ by Algorithm 2 and obtain $\{S_i\}_{i=1}^m$
4: **for** $k = 1 \rightarrow m$ **do**
5: sample n points $\{z_s^k\}$ in the region V_k
6: compute $\mathcal{L}_1^k = W(P_n|V_k, Q_n|S_k)$
7: $\mathcal{L}_2^k = \sum_{x \in \{x_t | z_t \in S_k\}} \|x - \psi(\phi(x))\|$
8: the local loss $\mathcal{L}_{local}^k = \mathcal{L}_1^k + \lambda \mathcal{L}_2^k$
9: compute $\mathcal{L}_3^k = W(P_n, Q_n)$, where P_n and Q_n are the empirical distributions of n random samples from Ω and $\{z_i\}_{i=1}^N$
10: $\mathcal{L}_4^k = \sum_{x \in \{x_t | z_t \in \text{supp } Q_n\}} \|x - \psi(\phi(x))\|$
11: the global loss $\mathcal{L}_{global}^k = \mathcal{L}_3^k + \lambda \mathcal{L}_4^k$
12: update ϕ and ψ by minimizing $\mathcal{L}^k = \mathcal{L}_{local}^k + \alpha(\mathcal{L}_{global}^k - \mathcal{L}_{global}^{k-1})$
13: **end for**
14: **until** convergence

optimization strategy is inspired by CEASE [23] and CSL [24] algorithms in distributed computing, where $f_i(\theta)$ is changed into $f(\theta)$ in each node machine under the assumption that data in different node machines are identically distributed. On the contrary, we assume the supports of distributions in different batches are disjoint, so we keep the first-order Taylor expansion unchanged to retain the differences. The algorithm of TWAE with regularization is summarized in **Algorithm 3**.

4 THEORETICAL ANALYSIS

From a statistical view, the estimation of discrepancy by the discriminator in GAN is biased and of high variance. Since the discriminator has cumulative preferences of features when classify real and fake data, the estimates of discrepancy are somehow biased. Moreover, as of two-player setting, noise impedes drastically more the training compared to single objective one [25]. Thus, the variance is high. On the contrary, non-adversarial methods treat each data equally and have low variance on estimating the discrepancy. However, since non-adversarial methods are not accurate enough and not over-parameterized to memorize data, they suffer from errors, which are analysable. Suppose P_N and Q_N are empirical distributions of the sampled data $\{\widehat{z}_i\}_{i=1}^N$ and encoded data $\{z_i\}_{i=1}^N$, while P_n and Q_n denote the empirical distributions of batches with n points sampled from $\{\widehat{z}_i\}_{i=1}^N$ and $\{z_i\}_{i=1}^N$, respectively. We use $\widehat{W}(\cdot, \cdot)$ to denote the estimator of the true Wasserstein distance $W(\cdot, \cdot)$, then the error of estimation can be divided into sample error e_s and measurement error e_m based on

$$\begin{aligned} \left| \widehat{W}(P_n, Q_n) - W(P_N, Q_N) \right| &\leq \left| W(P_n, Q_n) - W(P_N, Q_N) \right| \\ &\quad + \left| \widehat{W}(P_n, Q_n) - W(P_n, Q_n) \right| \\ &= e_s + e_m \end{aligned} \quad (24)$$

In the following, we will elaborate the superiority of the tessellation to reduce e_s and e_m respectively.

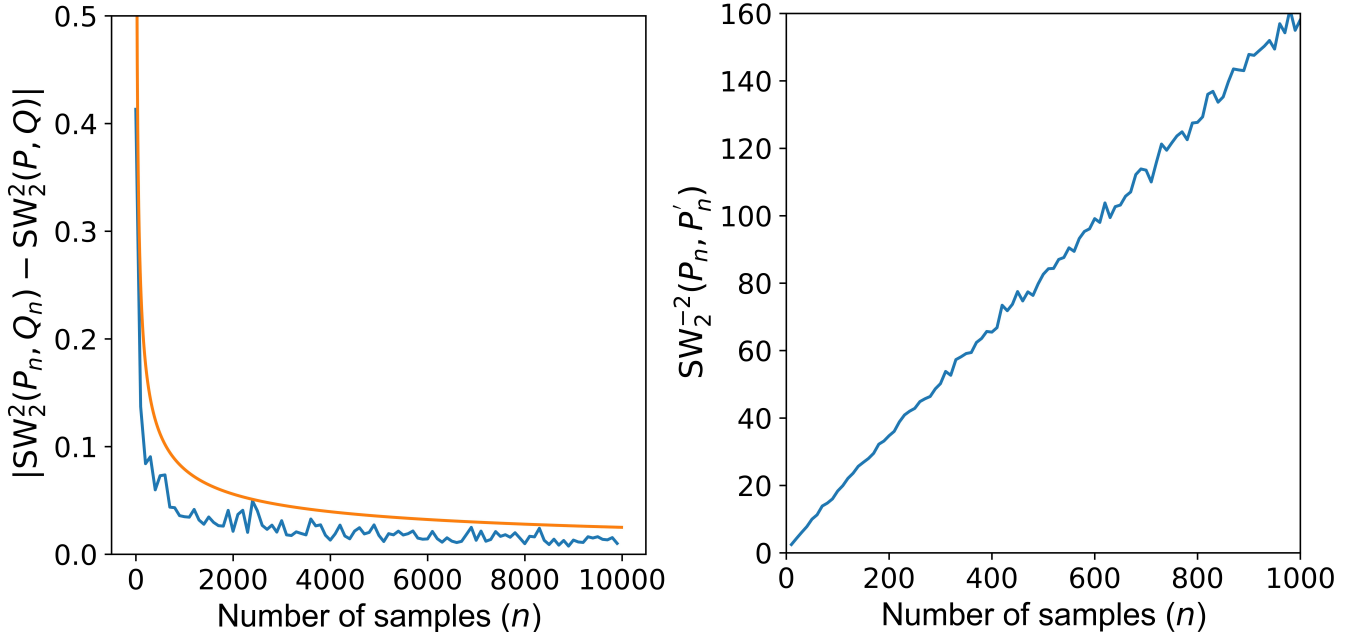


Fig. 2. Illustration of the asymptotic property of the sliced-Wasserstein (SW) distance. Here P_n and P'_n are sampled from the same Gaussian distribution P of 64-dimension. Q_n is sampled from a uniform distribution in the unit ball of 64-dimension. $|SW_2^2(P_n, Q_n) - SW_2^2(P, Q)|$ is bounded by the orange line of $\frac{C}{\sqrt{n}}$, while the reciprocal of SW distance $SW_2^{-2}(P_n, P'_n)$ increases linearly with n .

4.1 Sample Error

In practice, the size of data is too large to optimize, and we sample batches for better computation. Thus, the speed of convergence of the Wasserstein distance P_n to P_N is of importance. Sommerfeld and Munk [26] showed that the convergence rate is $n^{-\frac{1}{2}}$, i.e.,

Theorem 1. Suppose P is an empirical distribution. Let P_n be generated by i.i.d. samples $\tilde{z}_1, \dots, \tilde{z}_n \sim P$. Then with n approaching infinity

$$\sqrt{n}W_2^2(P_n, P) \rightarrow \gamma_1$$

where γ_1 is a random variable correlated with P .

The theorem indicates that the convergence rate of empirical distribution is independent of the dimension. So we need not worry about the curse of dimensionality. However, if P is absolutely continuous on R^d , then $\mathbb{E}[W_2(P_n, P)] > Cn^{-\frac{1}{d}}$ [27]. Since computation of the SW distance is based on empirical distribution and is equivalent to the Wasserstein distance. This asymptotic property can be generalized to the SW distance.

Theorem 2. Suppose P and Q are empirical distributions. Let P_n and Q_n be generated by i.i.d. samples $z_1, \dots, z_n \sim Q$ and $\tilde{z}_1, \dots, \tilde{z}_n \sim P$ respectively. P'_n is an independent copy of P_n . Then with n approaching infinity

$$\begin{aligned} \sqrt{n}(SW_2^2(P_n, Q_n) - SW_2^2(P, Q)) &\rightarrow N(0, \sigma^2) \\ nSW_2^2(P_n, P'_n) &\rightarrow \gamma_2 \end{aligned}$$

where σ^2 is the variance correlated with P and Q , and γ_2 is a random variable correlated with P .

Proof. For fixed $w \in S^{d-1}$, we first see the asymptotic property of Wasserstein distance in the one-dimensional space.

Let $P_{n|w}, P'_{n|w}, Q_{n|w}, P_w, Q_w$ be the projected empirical distributions of P_n, P'_n, Q_n, P and Q respectively. The results in [28] [29] showed that, with n approaching infinity,

$$\sqrt{n}(W_2^2(P_{n|w}, Q_{n|w}) - W_2^2(P_w, Q_w)) \rightarrow N(0, \sigma_1^2) \quad (25)$$

$$nW_2^2(P_{n|w}, P'_{n|w}) \rightarrow \gamma' \quad (26)$$

where $\sigma = \sigma(P, Q, w)$, $\gamma' = \gamma'(P, w)$. Since S^{d-1} is compact and by the definition of the SW distance, we obtain that, with n approaching infinity,

$$\sqrt{n}(SW_2^2(P_n, Q_n) - SW_2^2(P, Q)) \rightarrow \int_{w \in S^{d-1}} N(0, \sigma_1(w)^2) dw \quad (27)$$

$$nSW_2^2(P_n, P'_n) \rightarrow \int_{w \in S^{d-1}} \gamma'(w) dw \quad (28)$$

where $\int_{w \in S^{d-1}} N(0, \sigma_1(w)^2) dw$ is also gaussian, denoted by $N(0, \sigma^2)$, and $\int_{w \in S^{d-1}} \gamma'(w) dw$ is the random variable denoted by γ_2 . \square

Numerical test simulates the asymptotic property of the SW distance (Fig. 2) and we observe that $|SW_2^2(P_n, Q_n) - SW_2^2(P, Q)|$ and $SW_2^2(P_n, P'_n)$ decrease roughly via $\mathcal{O}(n^{-\frac{1}{2}})$ and $\mathcal{O}(n^{-1})$, respectively. Then we can obtain upper bounds correlated with n , which are tighter than Claim 1 in [14],

$$\mathbb{E}[|SW_2^2(P_n, Q_n) - SW_2^2(P, Q)|] \leq \frac{C_1}{\sqrt{n}} \quad (29)$$

$$\mathbb{E}[SW_2^2(P_n, P'_n)] \leq \frac{C_2}{n} \quad (30)$$

where C_1 and C_2 are two constants. For the GW distance, Rippl *et al.* proved a similar asymptotic property (Theorem 2.2 in [30])

Theorem 3. Let $P \neq Q$ be Gaussian, $P \sim N(m_1, \Sigma_1)$, $Q \sim N(m_2, \Sigma_2)$ with Σ_1 and Σ_2 having full rank. Let P_n and Q_n be generated by i.i.d. samples $z_1, \dots, z_n \sim Q$ and $\tilde{z}_1, \dots, \tilde{z}_n \sim P$, respectively. P'_n is an independent copy of P_n . Then with n approaching infinity

$$\sqrt{n} (GW^2(P_n, Q_n) - GW^2(P, Q)) \rightarrow N(0, w)$$

$$nGW^2(P_n, P'_n) \rightarrow \gamma_3$$

where w is correlated with P and Q , and γ_3 is correlated with P .

The target of generative models is to learn a continuous distribution. However, the road to continuity is discrete sampling. Points sampled randomly from the prior distribution are compared with the real data to make the encoder of auto-encoders or generator of GANs smooth in the latent space or the data space, respectively. Thus, while optimizing each batch, the task is to minimize the discrepancy of empirical distributions. Theorems 1, 2 and 3 give insights into why GANs perform better with larger batch sizes [31]. On the other hand, the size of batches in deep learning is limited by computational resources. TWAE solves this dilemma by sampling the same number of points from different Voronoi regions.

Suppose the whole support Ω of the prior distribution P_z is tessellated into m regions, and we utilize the SW distance to measure the discrepancy. On the one hand, if we sample n points in each region, there will be mn points on Ω in total. Then the sample error will be $\mathcal{O}(\frac{1}{\sqrt{mn}})$. On the other hand, if we sample n points from Ω for m times, then the error will be added up to $\mathcal{O}(\frac{m}{\sqrt{n}})$. In other words, if we optimize with batches of size n on Ω , then after a few epochs, $SW_2^2(P_n, Q_n)$ is approximately equal to $SW_2^2(P_n, P'_n)$, where P'_n is an independent copy of P_n . This means we can not identify Q_z from P_z with n sampled points. However, if we take a look at a region V_i with probability $P(V_i) = \frac{1}{m}$, we can still find differences between $P_{n|V_i}$ and $Q_{n|V_i}$ because in the past batches only a few points located in V_i and the sample error was high. So the local information is lost in this way. On the contrary, TWAE samples a batch from each region, so that with the same size of batches, we can approximate the continuous distribution better. Numerical experiments in Section 5 demonstrate the effectiveness of this idea.

4.2 Measurement Error

The SW and GW discrepancy metrics may lead to inaccurate estimation of the discrepancy. For the SW distance, we replace the integration in (8) over S^{d-1} with a summation over a randomly chosen set of unit vectors \hat{S}^{d-1} . For the GW distance, we approximate P_n and Q_n with Gaussian distributions. We expect that the sum of errors for measuring the discrepancies on the tessellated supports is smaller than that on the whole support. For instance, if we approximate $P_{n|V_j}$ with a Gaussian distribution in each region of Ω , we are actually utilizing a Gaussian mixture model to approximate P_N . A standard result in Bayesian nonparametrics says that every probability density is closely approximable by an infinite mixture of Gaussians. However, since the distribution can be arbitrarily complex, it is hard

to show the reduction of error with the increase of m . The measurement error induced by different approaches can be unified by utilizing a parameter ϵ to depict the estimator \widehat{W} . We assume that the expectation of P_n and Q_n is equal. Then it can be easily verified using the triangle inequality, i.e.,

$$\begin{aligned} W_2^2(P_n, Q_n) &= \min_{\sigma} \frac{1}{n} \sum_{i=1}^n \|z_i - \tilde{z}_{\sigma(i)}\|_2^2 \\ &\leq \frac{2}{n} \sum_{i=1}^n \|z_i - \mathbb{E}_{z \sim P_n}[z]\|_2^2 + \frac{2}{n} \sum_{i=1}^n \|\tilde{z}_i - \mathbb{E}_{z \sim Q_n}[z]\|_2^2 \quad (31) \\ &= \frac{2(n-1)}{n} [\text{tr}(\Sigma(P_n)) + \text{tr}(\Sigma(Q_n))] \end{aligned}$$

where $\Sigma(P_n)$, $\Sigma(Q_n)$ are the unbiased empirical covariance matrices of P_n and Q_n respectively, and $\text{tr}(\cdot)$ is the trace operator.

Definition 1. Suppose P and Q are empirical distributions. An estimator \widehat{W} is ϵ -good for (P, Q) if it holds that $|\widehat{W}_2^2(P, Q) - W_2^2(P, Q)| \leq \epsilon(\text{tr}(\Sigma(P)) + \text{tr}(\Sigma(Q)))$

For instance, while adopting the GW distance, we utilize multivariate Gaussians to approximate P and Q , and ignore the information in the moments higher than two. Intuitively, by doing Taylor expansion on $|\widehat{W}_2^2(P, Q) - W_2^2(P, Q)|$, the loss of moments higher than two can be bounded by the variance of P and Q . Then we obtain an upper bound to the measurement error of the tessellated Wasserstein distance, and prove the optimality of the usage of CVT according to the bound.

Theorem 4. Let P be a uniform distribution on Ω , $\{V_j\}_{j=1}^m$ be a tessellation on Ω . Q is the target distribution and \mathcal{T} is the optimal transportation map from P to Q . Assume \mathcal{T} is L -Lipschitz on Ω . $P_{n|V_j}$ and $Q_{n|\mathcal{T}(V_j)}$ are the empirical distributions of n points i.i.d. sampled from P restricted to V_j and Q restricted to $\mathcal{T}(V_j)$, respectively. The estimator \widehat{W} is ϵ -good for $\{(P_{n|V_j}, Q_{n|\mathcal{T}(V_j)})\}_{j=1}^m$. The estimate error of the tessellated Wasserstein distance is

$$\begin{aligned} \text{error} &= \sum_{i=1}^m P(V_i) |W_2^2(Q_{n|\mathcal{T}(V_i)}, P_{n|V_i}) \\ &\quad - \widehat{W}_2^2(Q_{n|\mathcal{T}(V_i)}, P_{n|V_i})| \end{aligned} \quad (32)$$

Then we have

$$\mathbb{E}[\text{error}] \leq \frac{\epsilon(1+L^2)}{|\Omega|} \sum_{i=1}^m \int_{V_i} \|z - \hat{z}_i\|_2^2 dz \quad (33)$$

where \hat{z}_i is the mass centroid of V_i . The right side of the inequation (33) can be viewed as a function of $\mathcal{F}(V, \hat{z})$. Furthermore, a necessary condition for the right side to be minimized is that V is the CVT and \hat{z} is the generator set.

Proof. For the ϵ -good estimator \widehat{W} , the error bound of the

tessellated Wasserstein distance is

$$\begin{aligned}
& \sum_{i=1}^m P(V_i) \left| W_2^2(Q_{n|\mathcal{T}(V_i)}, P_{n|V_i}) - \widehat{W}_2^2(Q_{n|\mathcal{T}(V_i)}, P_{n|V_i}) \right| \\
& \leq \epsilon \sum_{i=1}^m P(V_i) (\text{tr}(\Sigma(Q_{n|\mathcal{T}(V_i)})) + \text{tr}(\Sigma(P_{n|V_i}))) \\
& = \frac{\epsilon n}{n-1} \sum_{i=1}^m P(V_i) \mathbb{E}_{z \sim P_{n|V_i}} [\|\mathcal{T}(z) - \bar{\mathcal{T}}_i\|_2^2 + \|z - \bar{z}\|_2^2] \\
& \leq \frac{\epsilon n}{n-1} \sum_{i=1}^m P(V_i) (1 + L^2) \mathbb{E}_{z \sim P_{n|V_i}} [\|z - \bar{z}\|_2^2] \\
& = \frac{\epsilon n (1 + L^2)}{(n-1)|\Omega|} \sum_{i=1}^m |V_i| \mathbb{E}_{z \sim P_{n|V_i}} [\|z - \bar{z}\|_2^2]
\end{aligned} \tag{34}$$

where $\bar{z} = \mathbb{E}_{z \sim P_{n|V_i}}[z]$, $\bar{\mathcal{T}}_i = \mathbb{E}_{z \sim P_{n|V_i}}[\mathcal{T}(z)]$. The last equation is because $P(V_i) = \frac{|V_i|}{|\Omega|}$. Let $\tilde{z}_1^{(i)}, \dots, \tilde{z}_n^{(i)}$ be the support points of $P_{n|V_i}$, since they are randomly sampled from the uniform distribution on V_i , then

$$\begin{aligned}
\mathbb{E}_{P_{n|V_i}} [\mathbb{E}_{z \sim P_{n|V_i}} [\|z - \bar{z}\|_2^2]] &= \mathbb{E}_{P_{n|V_i}} \left[\frac{1}{n} \sum_{k=1}^n \|\tilde{z}_k^{(i)} - \bar{z}\|_2^2 \right] \\
&= \frac{n-1}{n|V_i|} \int_{V_i} \|z - \hat{z}_i\|_2^2 dz
\end{aligned} \tag{35}$$

where $\hat{z}_i = \frac{1}{|V_i|} \int_{V_i} z dz$. Taking it to (34), we obtain the upper bound in (33). Next, we will prove CVT is the necessary condition to minimize the upper bound.

First, fix the tessellation V , $\forall j \in \{1, \dots, m\}$

$$\int_{V_j} \|z - z_j^*\|_2^2 dz = \int_{V_j} (\|z\|_2^2 - 2z^T z_j^* + \|z_j^*\|_2^2) dz \tag{36}$$

The integration is minimized when $z_j^* = \hat{z}_j$. Second, fix \hat{z} and see what happens if V is not a Voronoi tessellation generated by \hat{z} . Suppose that \widehat{V} is the Voronoi tessellation generated by \hat{z} . Since V is not a Voronoi tessellation, there exists a particular value of $z \in V_i$, $\exists j \in \{1, \dots, m\}$ that

$$\|z - \hat{z}_j\|_2^2 < \|z - \hat{z}_i\|_2^2 \tag{37}$$

Thus,

$$\sum_{i=1}^m \int_{V_i} \|z - \hat{z}_i\|_2^2 dz > \sum_{i=1}^m \int_{\widehat{V}_i} \|z - \hat{z}_i\|_2^2 dz \tag{38}$$

So that the upper bound is minimized when V is chosen to be the CVT and \hat{z} is the set of generators. \square

Theorem 5. In the setting of Theorem 4. Assume

$$(V^*, \hat{z}^*) \in \arg \min_{V, \hat{z}} \mathcal{F}(V, \hat{z})$$

then

$$\mathcal{F}(V^*, \hat{z}^*) \leq \frac{\epsilon(1 + L^2) \mathbb{E} [C(P_{n|V_i^*}, i = 1, \dots, m)]}{\sqrt{m}}$$

which means, utilizing V^* as tessellation, the estimate error of tessellated Wasserstein distance is upper bounded,

$$\mathbb{E}[\text{error}] \leq \frac{\epsilon(1 + L^2) \mathbb{E} [C(P_{n|V_i^*}, i = 1, \dots, m)]}{\sqrt{m}}$$

Proof. Following the result in Theorem 4, we have

$$\begin{aligned}
\mathcal{F}(V^*, \hat{z}^*) &= \frac{\epsilon(1 + L^2)}{|\Omega|} \sum_{i=1}^m \int_{V_i^*} \|z - \hat{z}_i^*\|_2^2 dz \\
&= \frac{\epsilon(1 + L^2)}{|\Omega|} \sum_{i=1}^m |V_i^*| \mathbb{E}_{P_{n|V_i^*}} [\mathbb{E}_{z \sim P_{n|V_i^*}} [\|z - \hat{z}_i^*\|_2^2]]
\end{aligned} \tag{39}$$

Since $(V^*, \hat{z}^*) \in \arg \min_{V, \hat{z}} \mathcal{F}(V, \hat{z})$, following the result in Theorem 4, V^* is a CVT and \hat{z}^* is its generator. Let $P^* = \sum_{i=1}^m \frac{|V_i^*|}{|\Omega|} P_{n|V_i^*}$, $Q^* = \sum_{i=1}^m \frac{|V_i^*|}{|\Omega|} \delta_{\hat{z}_i^*}$. Suppose \mathcal{T}_1 is the optimal transportation map from P^* to Q^* , then $\forall z \in \text{supp } P_{n|V_i^*}$, $\mathcal{T}_1(z) = \hat{z}_i^*$, which is held for $i = 1, \dots, m$. Thus, we have

$$\sum_{i=1}^m \frac{|V_i^*|}{|\Omega|} \mathbb{E}_{P_{n|V_i^*}} [\mathbb{E}_{z \sim P_{n|V_i^*}} [\|z - \hat{z}_i^*\|_2^2]] = \mathbb{E}_{P^*} [W_2^2(P^*, Q^*)] \tag{40}$$

Since P^* is an empirical distribution, let P_m^* be an empirical distribution of m points i.i.d. sampled from P^* . Thus, following the results in Theorem 1 and combining this with (39) and (40), we have

$$\begin{aligned}
\mathcal{F}(V^*, \hat{z}^*) &= \epsilon(1 + L^2) \mathbb{E}_{P^*} [W_2^2(P^*, Q^*)] \\
&\leq \epsilon(1 + L^2) \mathbb{E}_{P^*} [\mathbb{E}_{P_m^*} [W_2^2(P^*, P_m^*)]] \\
&\leq \epsilon(1 + L^2) \mathbb{E}_{P^*} \left[\frac{C}{\sqrt{m}} \right]
\end{aligned} \tag{41}$$

where $C = C(P^*)$. \square

Since in the training procedure we need to define the tessellation V before Q is known, the upper bound of error corresponding to V is of importance. Theorem 4 gives the reason for utilizing the CVT technique and Theorem 5 shows that the error decrease with a rate of $m^{-\frac{1}{2}}$. Note that after a few iterations, Q is approximately equal to P , then the optimal transportation map \mathcal{T} is almost identical. Thus, $\mathcal{T}(V_i) \approx V_i$ is a set of points that are closest to \hat{z}_i other than \hat{z}_j ($j \neq i$). So the empirical distribution of S_i obtained by (15) is close to $Q_{n|\mathcal{T}(V_i)}$. Thus, in the algorithm, we compute $W(P_{n|V_i}, Q_{n|S_i})$ instead of $W(P_{n|V_i}, Q_{n|\mathcal{T}(V_i)})$. If $\{V_i\}_{i=1}^m$ is not a CVT, $Q_{n|\mathcal{T}(V_i)}$ and $Q_{n|S_i}$ will not coincide. The error induced by the approximation of $Q_{n|S_i}$ to $Q_{n|\mathcal{T}(V_i)}$ is hard to model. Nevertheless, it makes little effect on the results in the experiment.

5 EXPERIMENTAL RESULTS

In this section, we numerically evaluate TWAE from five aspects. In section 5.3, we compare TWAE with related studies. In section 5.4, we test the optimization method introduced in section 3. In section 5.5, we compare the performance of the CVT technique and sphere packing. Finally, in section 5.6, we compare the models with and without tessellation. We trained TWAE with the GW distance (TWAE-GW) and the SW distance (TWAE-SW) respectively on two real-world datasets including MNIST [32] consisting of 70k images and CelebA [33] consisting of about 203k images. We use the Fréchet inception distance (FID) introduced by [34] to measure the quality of the generated images. Smaller FID indicates better quality.

5.1 Architectures for different datasets

For the MNIST dataset, we use a simple auto-encoder consisting of a mirrored deep convolutional neural network with ReLU as the activation function to compare the performance of the CVT technique and sphere packing (Section 5.5).

Encoder architecture:

$$\begin{aligned} x \in \mathcal{R}^{28 \times 28} &\rightarrow \text{Conv}_{128} \rightarrow \text{BN} \rightarrow \text{ReLU} \\ &\rightarrow \text{Conv}_{256} \rightarrow \text{BN} \rightarrow \text{ReLU} \\ &\rightarrow \text{Conv}_{512} \rightarrow \text{BN} \rightarrow \text{ReLU} \\ &\rightarrow \text{Conv}_{1024} \rightarrow \text{BN} \rightarrow \text{ReLU} \rightarrow \text{FC}_8 \end{aligned}$$

Decoder architecture:

$$\begin{aligned} z \in \mathcal{R}^8 &\rightarrow \text{FC}_{7 \times 7 \times 1024} \\ &\rightarrow \text{FSConv}_{512} \rightarrow \text{BN} \rightarrow \text{ReLU} \\ &\rightarrow \text{FSConv}_{256} \rightarrow \text{BN} \rightarrow \text{ReLU} \rightarrow \text{FSConv}_1 \end{aligned}$$

For the CelebA dataset, we use two architectures A and B with different sizes of parameters to test if TWAE shows consistent results under different architectures (Fig. 3). Numerical experiments show that our tessellation technique is effective on both architectures. The FID score decreases rapidly when the number of regions m is lower than 100. However, there is no more decline when m is larger. Architecture A is similar to that of Tolstikhin *et al.* (2017) [3] and is used to compare the performance of TWAE with other generative auto-encoders fairly (Section 5.3).

Encoder of architecture A:

$$\begin{aligned} x \in \mathcal{R}^{64 \times 64 \times 3} &\rightarrow \text{Conv}_{128} \rightarrow \text{BN} \rightarrow \text{ReLU} \\ &\rightarrow \text{Conv}_{256} \rightarrow \text{BN} \rightarrow \text{ReLU} \\ &\rightarrow \text{Conv}_{512} \rightarrow \text{BN} \rightarrow \text{ReLU} \\ &\rightarrow \text{Conv}_{1024} \rightarrow \text{BN} \rightarrow \text{ReLU} \rightarrow \text{FC}_{64} \end{aligned}$$

Decoder of architecture A:

$$\begin{aligned} z \in \mathcal{R}^{64} &\rightarrow \text{FC}_{8 \times 8 \times 1024} \\ &\rightarrow \text{FSConv}_{512} \rightarrow \text{BN} \rightarrow \text{ReLU} \\ &\rightarrow \text{FSConv}_{256} \rightarrow \text{BN} \rightarrow \text{ReLU} \\ &\rightarrow \text{FSConv}_{128} \rightarrow \text{BN} \rightarrow \text{ReLU} \rightarrow \text{FSConv}_3 \end{aligned}$$

Architecture B has the same number of layers and half the number of nodes. For less computational cost, we use architecture B to investigate the properties of TWAE extensively (Sections 5.4 and 5.6).

Encoder of architecture B:

$$\begin{aligned} x \in \mathcal{R}^{64 \times 64 \times 3} &\rightarrow \text{Conv}_{64} \rightarrow \text{BN} \rightarrow \text{ReLU} \\ &\rightarrow \text{Conv}_{128} \rightarrow \text{BN} \rightarrow \text{ReLU} \\ &\rightarrow \text{Conv}_{256} \rightarrow \text{BN} \rightarrow \text{ReLU} \\ &\rightarrow \text{Conv}_{512} \rightarrow \text{BN} \rightarrow \text{ReLU} \rightarrow \text{Conv}_{64} \end{aligned}$$

Decoder of architecture B:

$$\begin{aligned} z \in \mathcal{R}^{64} &\rightarrow \text{FSConv}_{512} \rightarrow \text{BN} \rightarrow \text{ReLU} \\ &\rightarrow \text{FSConv}_{256} \rightarrow \text{BN} \rightarrow \text{ReLU} \\ &\rightarrow \text{FSConv}_{128} \rightarrow \text{BN} \rightarrow \text{ReLU} \\ &\rightarrow \text{FSConv}_{64} \rightarrow \text{BN} \rightarrow \text{ReLU} \rightarrow \text{FSConv}_3 \end{aligned}$$

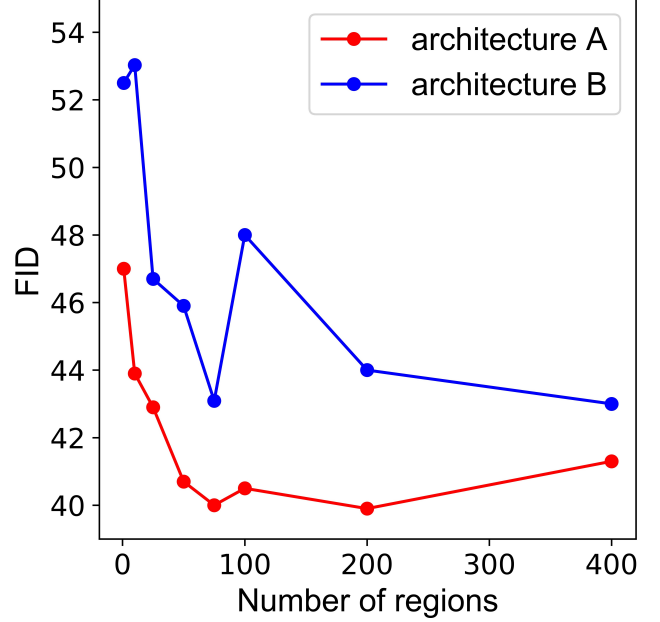


Fig. 3. Comparison of changing trend of FID scores versus the number of regions m . Here m are set to 1 (without tessellation), 10, 25, 50, 75, 100, 200, 400 for both architectures A and B.

5.2 Experimental setup

The hyperparameter λ of the auto-encoder in (10) is set to 1 for TWAE-SW and 0.01 for TWAE-GW. The dimensionalities of the latent space are set to 8 for MNIST and 64 for CelebA, respectively. The number 241 of root lattices of E_8 -lattice is chosen for sphere packing test. How many data points (N) in the training dataset are used for one single tessellation is a question. In the traditional setting, the data is shuffled in each epoch to prevent overfitting. If we take N as large as the size of the training dataset, the designed batches in each epoch will be approximately the same, which leads to bad generalization. Thus, larger N may not perform better. We tried various values of N and noticed that $N = 10000$ or 20000 work well for both MNIST and CelebA. Compared with traditional algorithms, the only extra computation is using LCM to solve the Hitchcock problem to design batches for each data. The time cost of LCM is only at most a few minutes for these settings before the model is optimized with N data points (Table 2). We implement our algorithms on Pytorch with the Adam optimizer.

5.3 TWAE can generate high-quality images

We first test if TWAE can approximate the support of the distribution of real data with a smooth and well-learned manifold by interpolations, test reconstruction, and random generating (Fig. 4). For interpolation, considering the probability concentrated near the surface of the unit ball, we interpolate on the curve near the surface instead of linear interpolation to avoid interpolating near the origin. In our experiments, the transition of the decoder from one point to another in the latent space is smooth and gradual. For reconstruction, TWAE can reconstruct the test data which means the model generalizes well. For random generating, samples are generated by sampling in the unit ball uniformly and

TABLE 1
Performance comparison of TWAE with or without regularizer on the MNIST and CelebA data with three given numbers of regions

| | MNIST | | | | CelebA | | | |
|-----------|---------|------------|---------|------------|---------|------------|---------|------------|
| | TWAE-SW | TWAE-SW(r) | TWAE-GW | TWAE-GW(r) | TWAE-SW | TWAE-SW(r) | TWAE-GW | TWAE-GW(r) |
| $m = 100$ | 20.4 | 16.3 | 18.0 | 15.9 | 49.2 | 47.8 | 46.7 | 44.5 |
| $m = 200$ | 17.5 | 16.0 | 15.7 | 14.3 | 50.2 | 44.1 | 47.2 | 48.1 |
| $m = 400$ | 15.6 | 13.9 | 14.2 | 13.8 | 47.2 | 43.5 | 54.0 | 57.2 |

TABLE 2
Time cost of LCM (seconds)

| | $m = 100$ | $m = 200$ | $m = 400$ |
|-------------|--------------|--------------|---------------|
| $N = 10000$ | 7.71 (0.02) | 24.34 (0.04) | 50.67 (0.16) |
| $N = 20000$ | 47.06 (0.01) | 96.56 (1.25) | 198.07 (1.27) |



Fig. 4. Comparison of interpolated, reconstructed and generated images by TWAE.

transforming the resulting vector z into an image via the decoder. By generating images of good quality, the “hole” in the latent space is filled and TWAE indeed generate a well-learned manifold. We also compared the performance of TWAE with WAE-GAN, WAE-MMD [3], SWAE [20] and

VAE [35]. Only WAE-GAN utilizes a discriminator. We use the results in [3], [20] since the architectures of these networks are similar, and it is not easy to reproduce the results of WAE-GAN. TWAE shows very competitive performance compared to WAE-GAN (Table 3).

TABLE 3
Performance comparison of different methods on the CelebA data

| Model | FID |
|---------|------|
| TWAE-SW | 39.9 |
| TWAE-GW | 44.5 |
| VAE | 63 |
| WAE-MMD | 55 |
| SWAE | 79 |
| WAE-GAN | 42 |

5.4 The non-identical batch optimization is effective

We set three different numbers of regions (i.e., $m = 100, 200, 400$) for both MNIST and CelebA datasets. Numerical results show that the FID score decreases with larger m on MNIST, while it doesn’t change significantly on CelebA (Table 1). The difference is probably due to the diverse complexity of the two datasets. We note that the distribution of each batch is different as we put similar data into a batch. The discrepancy of different batches is larger with relatively smaller batch sizes. To address this issue, we propose the non-identical batch optimization method (Section 3) by adding a regularizer (i.e., $\mathcal{L}_{global}^k - \mathcal{L}_{global}^{k-1}$ in **Algorithm 3**) for better generalization. Here the hyperparameter α is set to 0.2. Numerical results of TWAE with the regularizer indeed show better performance than without it with different m s for most cases (Table 1). The only exception is that for the GW distance with $m = 200$ and 400 respectively, which will be explained in Section 5.7.

5.5 The CVT technique gets similar performance with the exact model

The CVT technique is an iterative and approximate algorithm that can be adjusted to any dimensions. The iteration is based on integrating over each region. The computation goes up exponentially as the dimension increases. So the CVT technique may not be accurate enough in high-dimensional cases. Thus, it is necessary to explore the effect of it. We implement TWAE with exact lattices and compare its performance with that of the CVT technique. For the MNIST dataset, the dimension of the latent space is 8. Numerical results show that the CVT technique achieves comparable performance and gets very similar FID score

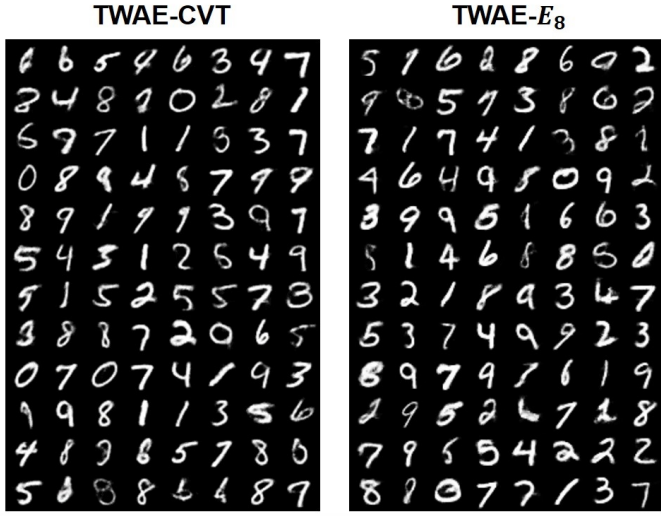


Fig. 5. Comparison of generated images of TWAE with CVT and E_8 -lattice. The FID scores of them are 16.8 and 16.9 respectively.

TABLE 4
Comparison of TWAE with and without tessellation

| distance (batch size) | with tessellation | without tessellation |
|-----------------------|-------------------|----------------------|
| SW (100) | 48.5 | 52.5 |
| SW (50) | 43.8 | 51.1 |
| SW (25) | 43.4 | 51.5 |
| GW (100) | 44.5 | 51.2 |
| GW (50) | 48.1 | 50.1 |
| GW (25) | 57.2 | 58.6 |

with the sphere packing E_8 -lattice dividing into 241 regions (Fig. 5), indicating that it gets similar performance with the exact model.

5.6 Tessellation indeed improve the performance of generation

Here we show that our tessellation procedure can indeed enhance the performance of non-adversarial methods using existing discrepancy metrics, such as the SW and GW distance. When utilize the GW distance without tessellation, we treat P_z and Q_z as multivariate Gaussian and ignore the information in the high-order moment. Thus, the approximation is not very good. But with the tessellation technique, actually, we are using a Gaussian mixture distribution with each component in a region to approximate the target distribution. With tessellation, it can be better than the state of the art non-adversarial auto-encoders. Furthermore, for the more accurate discrepancy metrics such as the SW distance, we achieve better performance (Table 4). In Fig. 6, we show the downward trends with and without tessellation in the training progress to prove that TWAE has superior generative performance, while keeping the good property of stability. However, for the SW distance, since the decoder of an auto-encoder is only trained with the reconstruction loss, it may not generalize to the “hole” between the training points. This means increasing the number of regions can not

go beyond the generalization ability of the decoder. For instance, the improvements from 200 regions to 400 regions is fewer than that from 100 regions to 200 regions. For the GW distance, when the batch size is smaller than the dimension of the latent space, the computation of $(\Sigma_2^{1/2} \Sigma_1 \Sigma_2^{1/2})^{1/2}$ in (4) is ill-posed. Consequently, the FID score doesn’t decrease notably as expected in the case of batch size = 50 and 25. Furthermore, TWAE is robust to the hyperparameter λ . In the case when λ is 100 times larger than default (Fig. 7), TWAE-GW can generate distinctly better images (FID=54.8) than without tessellation (FID=74.8).

In Fig. 8, we show that, at the end of the training procedure, the SW distance can not identify Q_n from P_n , i.e. $SW(Q_n, P_n)$ converges to $SW(P_n, P'_n)$, where P'_n is sampled from the same P_z as P_n . However, in the regions of the whole support, the discrepancy of P_z and Q_z still exists. With tessellation, the SW distance in the regions are closer to sampling from the same distribution, indicating that the tessellation could further reduces the discrepancy.

6 DISCUSSION AND CONCLUSION

In this paper, we propose a novel non-adversarial generative framework TWAE, which designs batches according to data similarity instead of random shuffling, and optimizes the discrepancy locally. It shows very competitive performance to an adversarial generative model WAE-GAN, while sharing the stability of other non-adversarial ones. It is very flexible and applicable to different discrepancy metrics to enhance their performance. To our knowledge, TWAE is the first generative model to design batches and optimize with non-identical distributions. To this end, we utilize a computational geometry technique CVT, which is often used in three-dimensional modeling, and develop a new optimization method to deal with such non-identical batches. TWAE can generate images of higher quality in terms of FID score with relatively more regions when the computing resource is adequate.

TWAE is designed to learn the data distribution in the latent space learned by an auto-encoder model, instead of the original space ($d > 1000$) of data (e.g., images). Generally, the distribution of data concentrates near a low-dimension manifold, so the similarity should be measured by the Riemann metric on the manifold rather than the Euclidean metric. However, construction of the Riemann metric in high dimensional space without neural network is hard. Thus, we suggest to tessellate the latent space to approximate the target distribution better. Here we suggest to use the uniform distribution but not the i.i.d. Gaussian as the prior distribution of the latent space. The reasons for this are threefold: 1) for a uniform distribution, the probability of a region $P(V_i)$ is corresponding to its volume. It is convenient to conduct tessellation with equal-weighted sampling; 2) uniform distribution is isotropic when restricted to a region. While computing the sliced-Wasserstein distance, projections of different directions will have useful information because the distribution is isotropic; 3) when the points obey uniform distribution, we can utilize the Euclidean metric to measure the similarity of two points.

Since the decoder ψ is trained on Q_z rather than P_z , the quality of generated images may not be as good as that of

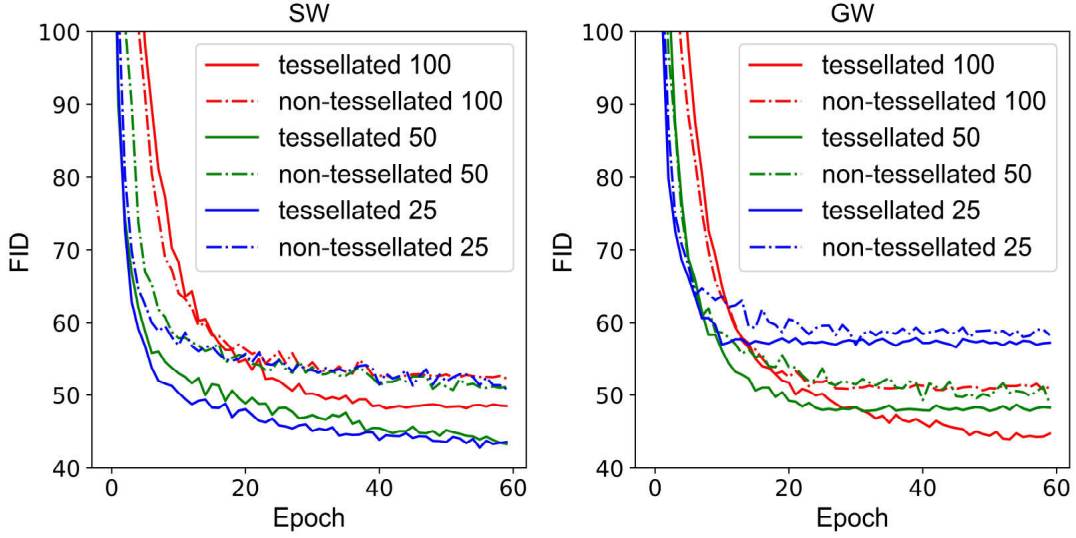


Fig. 6. Comparison of changing trend of FID scores versus training epochs between models with and without tessellation for both SW and GW distance. N is set to be 10000 in this experiment. $m = 100, 200, 400$ are used for tessellation, and correspondingly the batch sizes are set to 100, 50, 25 for models without tessellation, respectively.

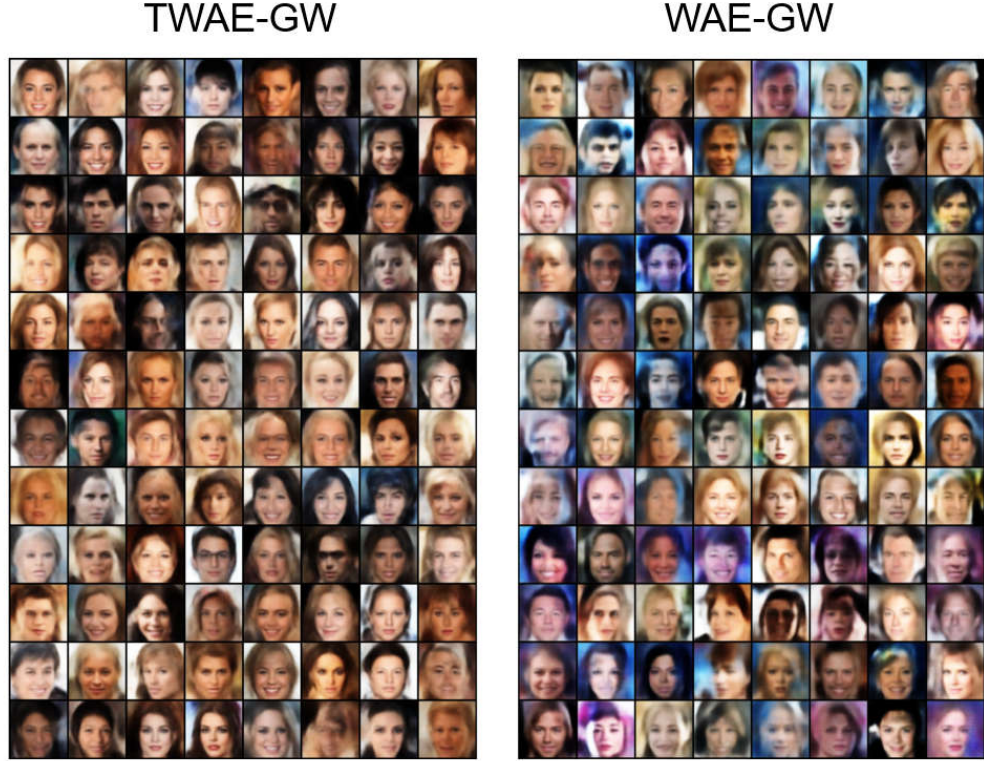


Fig. 7. Comparison of generated images using TWAE-GW and WAE-GW with $\lambda=1$ (100 times larger than default). The FID scores of TWAE-GW and WAE-GW are 54.8 and 74.8 respectively.

GAN. In some situations, people care about generating more than encoding. It is nontrivial to generalize the tessellation technique to GAN. The reason for this is two-fold: 1) The adversarial mechanism is unstable and sensitive to noise, thus the variance induced by such designed batches may impede the optimization process of GAN; 2) In GAN, there is no encoder to extract high-level representation of data, which makes it difficult to cluster the data into batches

according to their similarity. Nevertheless, it will be valuable to develop a technique analogous to tessellation that can enhance the performance of GAN.

In TWAE, since the supports of distributions of different batches are disjoint, the model will not forget the information in passed batches when learn with a new batch. However, neural network tends to forget the knowledge of previously learned tasks as information relevant to the

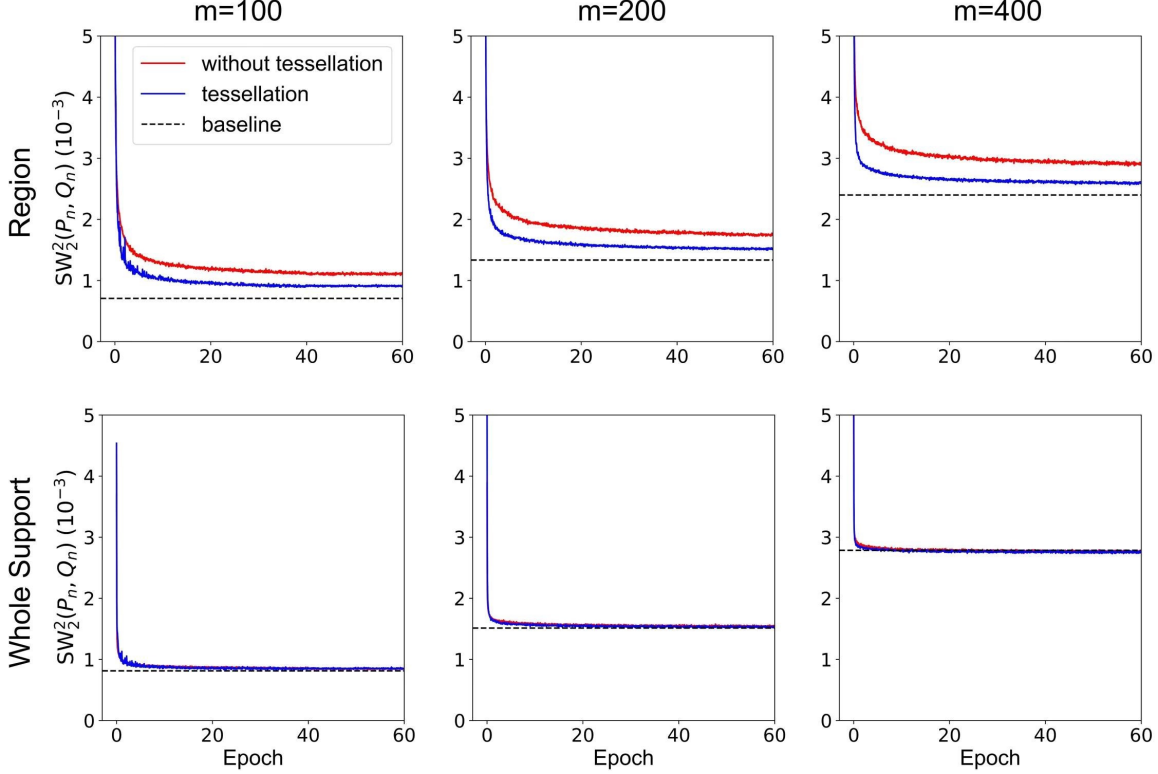


Fig. 8. Comparison of the SW distance in the training procedure with tessellation $m = 100, 200, 400$ and without tessellation. The baseline is the SW distance of two sets of points sampled from a uniform distribution in the unit ball (the whole support) or in the regions.

current task is incorporated. This phenomenon is termed catastrophic forgetting. For instance, in the situations of online machine learning, data becomes available in sequential order. So the distribution of each batch may change, and previously learned knowledge might lose. Numerical experiments showed that our optimization method can deal with non-identical batches, i.e. learning from the current batch without forgetting the former batches. Can techniques in catastrophic forgetting help to further reduce the gap of SW distance in the regions (Fig. 8)? Or can our non-identical batch optimization help to overcome the catastrophic forgetting? They will be valuable questions worthing further studying.

As mentioned above, the numbers of minimal vectors of E_8 -lattice and Leech lattice for 8- and 24-dimension cases are 240 and 196560 respectively. So the data we have actually can not fill the latent space when the dimension is very high. Some bad images will be generated when we randomly sample in the latent space due to the lack of data points. Unfortunately, there is no criterion to judge whether the sampled point in the latent space can generate a good image. In the future, how to build the statistics to evaluate the quality of the generated images and find the well-learned region in the latent space is an important topic.

ACKNOWLEDGMENTS

This work has been supported by the National Natural Science Foundation of China [11661141019, 61621003]; National Ten Thousand Talent Program for Young Top-notch Talents;

CAS Frontier Science Research Key Project for Top Young Scientist [QYZDB-SSW-SYS008].

REFERENCES

- [1] I. Goodfellow, J. Pouget-Abadie, M. Mirza, B. Xu, D. Warde-Farley, S. Ozair, A. Courville, and Y. Bengio, "Generative adversarial nets," in *Advances in neural information processing systems*, 2014, pp. 2672–2680.
- [2] A. Makhzani, J. Shlens, N. Jaitly, I. Goodfellow, and B. Frey, "Adversarial autoencoders," *arXiv preprint arXiv:1511.05644*, 2015.
- [3] I. Tolstikhin, O. Bousquet, S. Gelly, and B. Schoelkopf, "Wasserstein auto-encoders," *arXiv preprint arXiv:1711.01558*, 2017.
- [4] M. Arjovsky, S. Chintala, and L. Bottou, "Wasserstein gan," *arXiv preprint arXiv:1701.07875*, 2017.
- [5] M. Arjovsky and L. Bottou, "Towards principled methods for training generative adversarial networks. arxiv," 2017.
- [6] T. Salimans, I. Goodfellow, W. Zaremba, V. Cheung, A. Radford, and X. Chen, "Improved techniques for training gans," in *Advances in neural information processing systems*, 2016, pp. 2234–2242.
- [7] I. Goodfellow, "Nips 2016 tutorial: Generative adversarial networks," *arXiv preprint arXiv:1701.00160*, 2016.
- [8] T. Miyato, T. Kataoka, M. Koyama, and Y. Yoshida, "Spectral normalization for generative adversarial networks," *arXiv preprint arXiv:1802.05957*, 2018.
- [9] P. Isola, J.-Y. Zhu, T. Zhou, and A. A. Efros, "Image-to-image translation with conditional adversarial networks," in *Proceedings of the IEEE conference on computer vision and pattern recognition*, 2017, pp. 1125–1134.
- [10] M. Lucic, K. Kurach, M. Michalski, S. Gelly, and O. Bousquet, "Are gans created equal? a large-scale study," in *Advances in neural information processing systems*, 2018, pp. 700–709.
- [11] S. Arora, R. Ge, Y. Liang, T. Ma, and Y. Zhang, "Generalization and equilibrium in generative adversarial nets (gans)," in *Proceedings of the 34th International Conference on Machine Learning-Volume 70*. JMLR. org, 2017, pp. 224–232.

- [12] C.-L. Li, W.-C. Chang, Y. Cheng, Y. Yang, and B. Póczos, "Mmd gan: Towards deeper understanding of moment matching network," in *Advances in Neural Information Processing Systems*, 2017, pp. 2203–2213.
- [13] N. Bonnotte, "Unidimensional and evolution methods for optimal transportation," Ph.D. dissertation, Paris 11, 2013.
- [14] I. Deshpande, Z. Zhang, and A. G. Schwing, "Generative modeling using the sliced wasserstein distance," in *Proceedings of the IEEE Conference on Computer Vision and Pattern Recognition*, 2018, pp. 3483–3491.
- [15] N. Bonnotte, "From knothe's rearrangement to brenier's optimal transport map," *SIAM Journal on Mathematical Analysis*, vol. 45, no. 1, pp. 64–87, 2013.
- [16] L. V. Kantorovich, "On a problem of monge," *Journal of Mathematical Sciences*, vol. 133, no. 4, pp. 1383–1383, 2006.
- [17] I. Olkin and F. Pukelsheim, "The distance between two random vectors with given dispersion matrices," *Linear Algebra and its Applications*, vol. 48, pp. 257–263, 1982.
- [18] C. Villani, *Optimal transport: old and new*. Springer Science & Business Media, 2008, vol. 338.
- [19] I. Gulrajani, F. Ahmed, M. Arjovsky, V. Dumoulin, and A. C. Courville, "Improved training of wasserstein gans," in *Advances in neural information processing systems*, 2017, pp. 5767–5777.
- [20] S. Kolouri, P. E. Pope, C. E. Martin, and G. K. Rohde, "Sliced-wasserstein autoencoder: an embarrassingly simple generative model," *arXiv preprint arXiv:1804.01947*, 2018.
- [21] Q. Du, V. Faber, and M. Gunzburger, "Centroidal voronoi tessellations: Applications and algorithms," *SIAM review*, vol. 41, no. 4, pp. 637–676, 1999.
- [22] R. L. Griess Jr, "The e8-lattice, the leech lattice and beyond," *Ann Arbor*, vol. 1001, p. 48109.
- [23] J. Fan, Y. Guo, and K. Wang, "Communication-efficient accurate statistical estimation," *arXiv preprint arXiv:1906.04870*, 2019.
- [24] M. I. Jordan, J. D. Lee, and Y. Yang, "Communication-efficient distributed statistical inference," *Journal of the American Statistical Association*, vol. 114, no. 526, pp. 668–681, 2019.
- [25] T. Chavdarova, G. Gidel, F. Fleuret, and S. Lacoste-Julien, "Reducing noise in gan training with variance reduced extragradient," *arXiv preprint arXiv:1904.08598*, 2019.
- [26] M. Sommerfeld and A. Munk, "Inference for empirical wasserstein distances on finite spaces," *Journal of the Royal Statistical Society: Series B (Statistical Methodology)*, vol. 80, no. 1, pp. 219–238, 2018.
- [27] J. Weed, F. Bach *et al.*, "Sharp asymptotic and finite-sample rates of convergence of empirical measures in wasserstein distance," *Bernoulli*, vol. 25, no. 4A, pp. 2620–2648, 2019.
- [28] E. Del Barrio, J. A. Cuesta-Albertos, C. Matrán, S. Csörgö, C. M. Cuadras, T. de Wet, E. Giné, R. Lockhart, A. Munk, and W. Stute, "Contributions of empirical and quantile processes to the asymptotic theory of goodness-of-fit tests," *Test*, vol. 9, no. 1, pp. 1–96, 2000.
- [29] A. Munk and C. Czado, "Nonparametric validation of similar distributions and assessment of goodness of fit," *Journal of the Royal Statistical Society: Series B (Statistical Methodology)*, vol. 60, no. 1, pp. 223–241, 1998.
- [30] T. Rippl, A. Munk, and A. Sturm, "Limit laws of the empirical wasserstein distance: Gaussian distributions," *Journal of Multivariate Analysis*, vol. 151, pp. 90–109, 2016.
- [31] A. Brock, J. Donahue, and K. Simonyan, "Large scale gan training for high fidelity natural image synthesis," *arXiv preprint arXiv:1809.11096*, 2018.
- [32] Y. LeCun, L. Bottou, Y. Bengio, P. Haffner *et al.*, "Gradient-based learning applied to document recognition," *Proceedings of the IEEE*, vol. 86, no. 11, pp. 2278–2324, 1998.
- [33] Z. Liu, P. Luo, X. Wang, and X. Tang, "Deep learning face attributes in the wild," in *Proceedings of the IEEE international conference on computer vision*, 2015, pp. 3730–3738.
- [34] M. Heusel, H. Ramsauer, T. Unterthiner, B. Nessler, and S. Hochreiter, "Gans trained by a two time-scale update rule converge to a local nash equilibrium," in *Advances in Neural Information Processing Systems*, 2017, pp. 6626–6637.
- [35] D. P. Kingma and M. Welling, "Auto-encoding variational bayes," *arXiv preprint arXiv:1312.6114*, 2013.